

ARTICLE

Received 25 Nov 2015 | Accepted 1 Apr 2016 | Published 3 May 2016

DOI: 10.1038/ncomms11488

OPEN

# Semi-metallic $\text{Be}_5\text{C}_2$ monolayer global minimum with quasi-planar pentacoordinate carbons and negative Poisson's ratio

Yu Wang<sup>1</sup>, Feng Li<sup>1</sup>, Yafei Li<sup>1</sup> & Zhongfang Chen<sup>2</sup>

Designing new materials with novel topological properties and reduced dimensionality is always desirable for material innovation. Here we report the design of a two-dimensional material, namely  $\text{Be}_5\text{C}_2$  monolayer on the basis of density functional theory computations. In  $\text{Be}_5\text{C}_2$  monolayer, each carbon atom binds with five beryllium atoms in almost the same plane, forming a quasi-planar pentacoordinate carbon moiety.  $\text{Be}_5\text{C}_2$  monolayer appears to have good stability as revealed by its moderate cohesive energy, positive phonon modes and high melting point. It is the lowest-energy structure with the  $\text{Be}_5\text{C}_2$  stoichiometry in two-dimensional space and therefore holds some promise to be realized experimentally.  $\text{Be}_5\text{C}_2$  monolayer is a gapless semiconductor with a Dirac-like point in the band structure and also has an unusual negative Poisson's ratio. If synthesized,  $\text{Be}_5\text{C}_2$  monolayer may find applications in electronics and mechanics.

<sup>1</sup>College of Chemistry and Materials Science, Jiangsu Key Laboratory of Biofunctional Materials, Nanjing Normal University, Nanjing, Jiangsu 210023, China.

<sup>2</sup>Department of Chemistry, Institute for Functional Nanomaterials, University of Puerto Rico, Rio Piedras Campus, San Juan, Puerto Rico 00931, USA.

Correspondence and requests for materials should be addressed to Y.L. (email: liyafei.abc@gmail.com) or to Z.C. (email: zhongfangchen@gmail.com).

Carbon in known molecules and materials typically has tetrahedral tetracoordination (for example, diamond), planar tricoordination (for example, graphite) or linear dicoordination (for example, ethyne) arrangements. Especially, the tetrahedral preference of tetracoordinate carbon compounds, which was deduced by van't Hoff<sup>1</sup> and Lebel<sup>2</sup> more than a century ago, is one of the major foundations of organic chemistry. In 1968, Monkhorst<sup>3</sup> first discussed an exceptional bonding pattern of carbon, namely planar tetracoordinate carbon (ptC), by proposing a planar methane ( $D_{4h}$ ), which is actually not a minimum energy structure. Later in 1970, by insightful analysis of ptC bonding in the hypothetical planar methane, Hoffman *et al.*<sup>4</sup> suggested that ptCs can be stabilized electronically by replacing H atoms in planar methane by  $\sigma$  donors (to facilitate electron transfer to electron-deficient  $\sigma$  bonds) or  $\pi$  acceptors (to delocalize the unfavourable lone pair of ptC). Along this line, in 1976 Collins *et al.*<sup>5</sup> theoretically devised the first ptC-containing molecule 1, 1-dilithiocyclopropane. One year later Cotton and Millar<sup>6</sup> synthesized the first ptC-containing molecule, although the unique ptC configuration was not recognized at that time. Ever since, ptC chemistry has been a subject of extensive studies<sup>7–9</sup>. Numerous ptC species have been designed theoretically<sup>10–15</sup> and some global minimum structures, such as  $CaI_4^+$  (ref. 16),  $CaI_4^{2+}$  (ref. 17) and  $CaI_3Si^-$  (ref. 18) have been observed experimentally. More excitingly, besides ptC, many molecules containing planar pentacoordinate carbon (ppC)<sup>19–22</sup> and hexacoordinate carbon (phC)<sup>23–25</sup> have been designed computationally. The rule-breaking chemical bonding in these planar hypercoordinate carbons can lead to completely new molecules and materials, which are of fundamental importance to chemistry and materials science.

The unique topology and dimensionality may lead to exceptional properties of materials. It is not a surprise to witness the growing interest in designing ptC-containing solids and nanostructures in recent years<sup>26–30</sup>. Especially, stimulated by the extensive studies of graphene<sup>31,32</sup> and inorganic layered materials<sup>33,34</sup>, many two-dimensional (2D) materials with rule-breaking chemical bonding have been designed computationally<sup>35–42</sup>. For example, on the basis of ptC molecule  $CB_4$  (ref. 43), Wu *et al.*<sup>35</sup> designed the first ptC-containing 2D material, namely  $B_2C$  graphene, which was later confirmed to be only a local minimum<sup>44</sup>. Li *et al.*<sup>36</sup> and Dai *et al.*<sup>37</sup> predicted that  $Al_2C$  monolayer in its lowest-energy configuration have all C atoms being ideal ptC. More interestingly, Li *et al.*<sup>45</sup> demonstrated recently that one C atom can bind to six beryllium (Be) atoms in an almost planar manner, yielding a phC-featuring 2D material with a  $Be_2C$  stoichiometry. With intriguing structural and electronic properties, these 2D materials are expected to have important applications in some specific fields.

In contrast to ptC and phC, no attempt exists for extending ppC into solids until now. Motivated by the successful design of ptC- and phC-containing materials, we are quite curious whether it is possible to extend ppC into solids. Addressing this issue would deliver not only unique structures but also some fantastic properties, which is of both theoretical and practical importance.

In this work, by means of density functional theory (DFT) computations, we first confirm that the ppC molecule  $Be_9C_2^{4-}$  is a local minimum on the potential energy surface. Based on the structural characters of  $Be_9C_2^{4-}$ , we design a ppC-containing 2D material, namely  $Be_5C_2$  monolayer, in which each C atom binds to five Be atoms to form a quasi-planar pentacoordinate moiety. Our  $Be_5C_2$  monolayer has rather good thermal and kinetic stabilities and is energetically the most favourable isomer in 2D space. Dramatically, the electronic band structure of  $Be_5C_2$  monolayer has a Dirac-like point at the Fermi level, endowing an

intriguing semimetallic feature. More interestingly,  $Be_5C_2$  monolayer possesses a negative Poisson's ratio, which is rather rare in nanostructures. These fascinating properties make  $Be_5C_2$  monolayer a promising candidate for future applications in electronics and mechanics.

## Results

**$Be_9C_2^{4-}$  as the inspiring ppC species for 2D monolayer.** Our design of periodic 2D  $Be_5C_2$  monolayer is initially inspired by our finding of the ppC molecule, namely  $Be_9C_2^{4-}$ , which has singlet ground state and  $D_{2h}$  symmetry (Fig. 1a). Computed at B3LYP level of theory with 6–311 +  $G^*(d, p)$  basis set,  $Be_9C_2^{4-}$  is a local minimum with the lowest vibrational frequency of  $158.5\text{ cm}^{-1}$ . In this molecule, each C atom binds to five Be atoms to form a ppC moiety of  $Be_5C$ , which has been shown to be a local minima<sup>20</sup>. Structurally,  $Be_9C_2^{4-}$  can be viewed as two  $Be_5C$  moieties fused by sharing one Be atom. The C–Be bond lengths are in the range of 1.70–1.76 Å, whereas the Be–Be bond lengths are in the range of 2.02–2.39 Å.

According to the natural population analysis, each ppC of  $Be_9C_2^{4-}$  possesses a 2.18 |e| negative charge ( $-0.40$  |e| according to the Hirshfeld charge population analysis) and the natural electron configuration is  $2s^{1.42}2p_x^{1.47}2p_y^{1.66}2p_z^{1.60}$ , indicating that ppCs in  $Be_9C_2^{4-}$  are essentially stabilized through Be  $\sigma$ -donation and delocalization of carbon  $2p_z$  electrons. The computed Wiberg bond index for C–Be bonds are 0.52 and 0.61, respectively, resulting in a total Wiberg bond index of 2.81 for each ppC. Moreover, we also scrutinized the molecular orbitals of  $Be_9C_2^{4-}$  to get more information on its stabilization mechanism. As shown in Fig. 1b, the highly delocalized  $\pi$  (for example, HOMO-7 and HOMO-8) and  $\sigma$  (for example, HOMO-3,

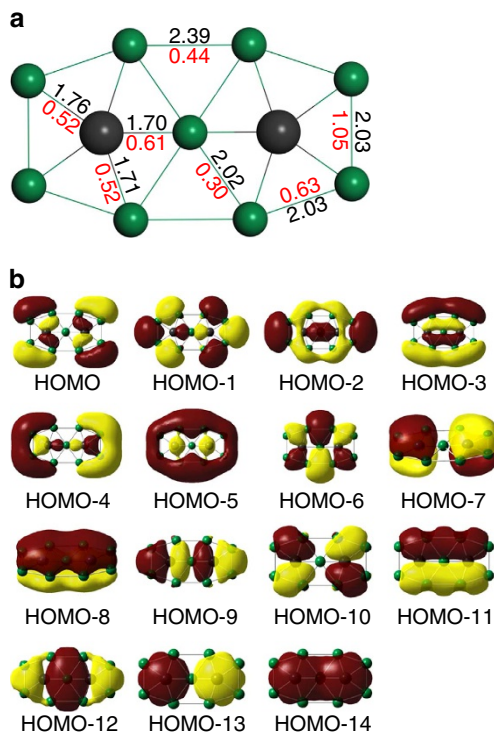


**Figure 1 |  $Be_9C_2^{4-}$  molecule.** (a) Optimized geometric structure of  $Be_9C_2^{4-}$  molecule. The black and green balls represent C and Be atoms, respectively. The red and black numbers are the Wiberg bond index (WBI) and lengths (in angstroms) of the representative chemical bonds, respectively. (b) The canonical molecular orbitals of  $Be_9C_2^{4-}$ .

HOMO-4 and HOMO-5) orbitals can help maintain the planar configuration.

**Geometric properties of Be<sub>5</sub>C<sub>2</sub> monolayer.** The fusing of two Be<sub>5</sub>C moieties to Be<sub>9</sub>C<sub>2</sub><sup>4-</sup> reminds us of the roadmap of fusing benzene rings to polycyclic aromatic hydrocarbons (for example, naphthalene and anthracene) and then to 2D infinite graphene. Inspired by the ppC-containing Be<sub>9</sub>C<sub>2</sub><sup>4-</sup>, we designed a new 2D inorganic material, namely Be<sub>5</sub>C<sub>2</sub> monolayer by generalizing the structural characters of Be<sub>9</sub>C<sub>2</sub><sup>4-</sup>. As shown in Fig. 2a, 1 unit cell of Be<sub>5</sub>C<sub>2</sub> monolayer consists of 8 C atoms and 20 Be atoms with the optimized lattice parameters being  $a = 8.92 \text{ \AA}$  and  $b = 9.21 \text{ \AA}$ , respectively. Similar to Be<sub>9</sub>C<sub>2</sub><sup>4-</sup>, in Be<sub>5</sub>C<sub>2</sub> monolayer each C atom binds to five Be atoms to form a ppC moiety of Be<sub>5</sub>C and two neighbouring Be<sub>5</sub>C moieties share one Be atom (Be<sub>1</sub>) to form a Be<sub>9</sub>C<sub>2</sub> moiety in the  $a$  (Be<sub>9</sub>C<sub>2</sub>-I) or  $b$  (Be<sub>9</sub>C<sub>2</sub>-II) direction. Especially, one Be<sub>9</sub>C<sub>2</sub>-I moiety is fused with four neighbouring Be<sub>9</sub>C<sub>2</sub>-II moieties by sharing the peripheral Be atoms (Be<sub>2</sub>) and *vice versa*, leading to the formation of a 2D network with four Be<sub>9</sub>C<sub>2</sub> moieties in one unit cell. The optimized coordinates of Be<sub>5</sub>C<sub>2</sub> monolayer are presented in Supplementary Table 1. It is noteworthy that the Be<sub>5</sub>C<sub>2</sub> monolayer is remarkably buckled rather than an exactly planar structure (Fig. 2b). The buckling, measured by the vertical distance between the bottommost Be atoms and the uppermost Be atom, is as high as 2.14 Å. Even so, the ppCs in Be<sub>5</sub>C<sub>2</sub> monolayer still have a good planarity (Supplementary Fig. 1). According to our computations, the total degrees of five Be–C–Be angles for ppCs in Be<sub>9</sub>C<sub>2</sub>-I and Be<sub>9</sub>C<sub>2</sub>-II moieties are 371.44° and 364.84°, respectively, which are a little higher than the ideal 360°. Interestingly, when Be<sub>9</sub>C<sub>2</sub><sup>4-</sup> is neutralized by four protons (H<sup>+</sup>), the obtained Be<sub>9</sub>C<sub>2</sub>H<sub>4</sub> molecule is also severely buckled (Supplementary Fig. 2). In Be<sub>5</sub>C<sub>2</sub> monolayer, the length of C–Be<sub>1</sub> bonds (1.66 Å, 1.68 Å) is much shorter than that of C–Be<sub>2</sub> bonds (1.73 Å, 1.74 Å). Moreover, our computations revealed that Be<sub>5</sub>C<sub>2</sub> monolayer has a non-magnetic ground state, indicating that there are no unpaired electrons in Be<sub>5</sub>C<sub>2</sub> monolayer.

We then computed the deformation electronic density of Be<sub>5</sub>C<sub>2</sub> monolayer to elucidate its bonding nature. The deformation electronic density is defined as the total electronic density excluding those of isolated atoms. As clearly shown in Fig. 2c,

some electrons are extracted from the 2s orbitals of Be atoms and well delocalized over C–Be bonds, indicating that C atoms form multicentre covalent bonds with neighbouring Be atoms, which is crucial for stabilizing the ppC moieties. The similar stabilizing mechanism has been found in pTC- and pHC-containing 2D materials<sup>35–40,45</sup>. According to the Hirshfeld charge popular analysis, C, Be<sub>1</sub> and Be<sub>2</sub> atoms in Be<sub>5</sub>C<sub>2</sub> monolayer possess a  $-0.32$ ,  $+0.16$  and  $+0.12$  |e| charge, respectively. The buckling of Be<sub>5</sub>C<sub>2</sub> monolayer stretches the Be–Be distances and probably helps reduce the otherwise even stronger repulsive interactions between Be atoms.

We also used the recently developed Solid State Adaptive Natural Density Partitioning (SSAdNDP) method<sup>46</sup> to better understand the unique chemical bonding of Be<sub>5</sub>C<sub>2</sub> monolayer. According to our results (Supplementary Fig. 3), there is no classical two-centre-two-electron (2c–2e) C–Be bond in Be<sub>5</sub>C<sub>2</sub> monolayer. For one unit cell of Be<sub>5</sub>C<sub>2</sub> monolayer, the SSAdNDP search revealed twenty-four 3c–2e Be–C–Be  $\sigma$ -bonds (responsible for the bonding within the Be<sub>5</sub>C units), four 4c–2e  $\sigma$ -bonds on four Be squares and eight 6c–2e  $\pi$ -bonds over eight Be<sub>5</sub>C units, accounting for 72 electrons per unit cell. This bonding pattern is consistent with the symmetry of Be<sub>5</sub>C<sub>2</sub> monolayer. Especially, the existence of delocalized  $\sigma$ - and  $\pi$ -bonds could essentially stabilize the ppCs in Be<sub>5</sub>C<sub>2</sub> monolayer.

**Stability of Be<sub>5</sub>C<sub>2</sub> monolayer.** Although Be<sub>5</sub>C<sub>2</sub> monolayer has rather intriguing structural properties, we are unclear whether it is a stable structure. To assess the stability, we first computed the cohesive energy of Be<sub>5</sub>C<sub>2</sub> monolayer, which is defined as:  $E_{\text{coh}} = (nE_{\text{C}} + mE_{\text{Be}} - E_{\text{Be}_5\text{C}_2}) / (n + m)$ , in which  $E_{\text{C}}$ ,  $E_{\text{Be}}$  and  $E_{\text{Be}_5\text{C}_2}$  are the total energies of a single C atom, a single Be atom and Be<sub>5</sub>C monolayer, respectively;  $n$  and  $m$  are the number of C and Be atoms in the supercell, respectively. According to our computations, Be<sub>5</sub>C<sub>2</sub> monolayer has a cohesive energy of 4.58 eV per atom. As a reference, the cohesive energies of the experimentally realized 2D silicene<sup>47,48</sup> and phosphorene<sup>49,50</sup> are 3.71 and 3.61 eV per atom, respectively. As silicene and phosphorene are composed of covalent bonds, the even higher cohesive energy can ensure that Be<sub>5</sub>C<sub>2</sub> monolayer is a strongly connected network.

The stability of Be<sub>5</sub>C<sub>2</sub> monolayer can be further confirmed by its phonon dispersion curves. As shown in Fig. 3a, no appreciable

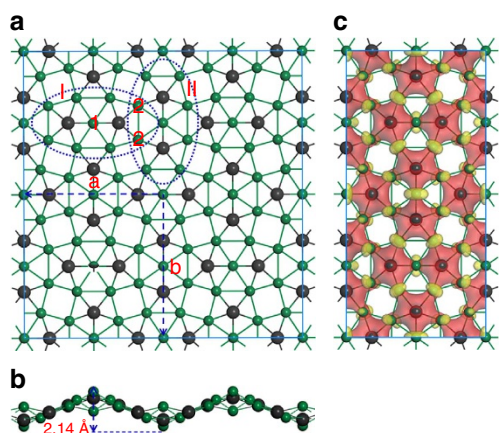


**Figure 2 | Geometric and electronic structures of Be<sub>5</sub>C<sub>2</sub> monolayer.**

(a) Top and (b) side views of geometric structure of Be<sub>5</sub>C<sub>2</sub> monolayer. The blue dashed lines denote a unit cell; a and b represent the lattice vectors, 1 and 2 denote the different Be atoms, I and II represent the different Be<sub>9</sub>C<sub>2</sub> moieties. (c) Deformation charge density of 2D Be<sub>5</sub>C<sub>2</sub> monolayer. Red and yellow refer to electron accumulation and depletion regions, respectively.

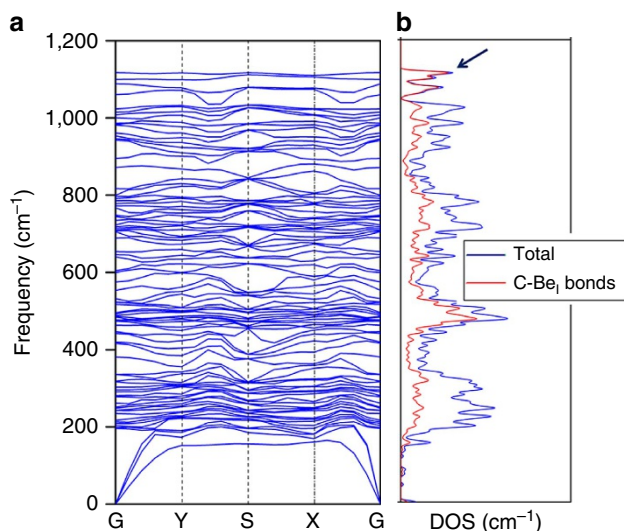


**Figure 3 | Kinetic stability of Be<sub>5</sub>C<sub>2</sub> monolayer.** (a) Phonon spectrum and (b) phonon DOS of Be<sub>5</sub>C<sub>2</sub> monolayer.

imaginary phonon mode is present, suggesting the good kinetic stability of  $\text{Be}_5\text{C}_2$  monolayer. Remarkably, the highest frequency of  $\text{Be}_5\text{C}_2$  monolayer reaches up to  $1,120\text{ cm}^{-1}$ , which is higher than those of  $\text{MoS}_2$  monolayer ( $473\text{ cm}^{-1}$ )<sup>51</sup>, silicene ( $580\text{ cm}^{-1}$ )<sup>52</sup> and our recently designed phC-containing  $\text{Be}_2\text{C}$  monolayer ( $1,020\text{ cm}^{-1}$ )<sup>45</sup>, indicating robust C–Be bonds in  $\text{Be}_5\text{C}_2$  monolayer. The analysis of partial phonon density of states (DOS; Fig. 3b) revealed that the highest frequency of  $\text{Be}_5\text{C}_2$  monolayer is mainly contributed by C–Be<sub>1</sub> bonds.

Moreover, to examine the thermal stability of  $\text{Be}_5\text{C}_2$  monolayer, we performed first-principles molecular dynamic (FPMD) simulations using a  $2 \times 2$  supercell. Our three simulations at temperature of 1,000, 1,500 and 2,000 K show that  $\text{Be}_5\text{C}_2$  monolayer can maintain its structural integrity throughout a 10-ps FPMD simulation up to 1,500 K, but is seriously disrupted at 2,000 K, suggesting that  $\text{Be}_5\text{C}_2$  monolayer has a melting point between 1,500 and 2,000 K (Supplementary Fig. 4). We also performed optimizations for the distorted structures from MD simulations. After full atomic relaxation, those structures from MD simulations at 1,000 and 1,500 K can recover the initial configuration of  $\text{Be}_5\text{C}_2$  monolayer. The above results demonstrate that  $\text{Be}_5\text{C}_2$  monolayer has a remarkable thermal stability.

The moderate cohesive energy, all positive phonon modes and good thermal stability can ensure that  $\text{Be}_5\text{C}_2$  monolayer is at least a local minimum structure on the potential energy surface. However, is the ppC-containing  $\text{Be}_5\text{C}_2$  monolayer a global minimum? It is noteworthy that the global minimum structure is more likely to be achieved than the local minimum structures experimentally. For example, many isomers of graphene, such as Haeckelite graphene<sup>53</sup>, T-graphene<sup>54</sup> and penta-graphene<sup>55</sup> have been designed computationally, but none of them has been realized experimentally. Therefore, we performed a global search for the lowest-energy structure of  $\text{Be}_5\text{C}_2$  monolayer in the 2D space using first-principles-based particle-swarm optimization (PSO) method as implemented in CALYPSO code. After a comprehensive search, we obtained three stable isomers of 2D  $\text{Be}_5\text{C}_2$ , which are labelled as  $\text{Be}_2\text{C}_5$ -I,  $\text{Be}_2\text{C}_5$ -II and  $\text{Be}_2\text{C}_5$ -III, respectively. As shown in Fig. 4a,  $\text{Be}_2\text{C}_5$ -I is actually the above discussed ppC-featuring  $\text{Be}_5\text{C}_2$  monolayer. Interestingly, in  $\text{Be}_2\text{C}_5$ -II (Fig. 4b) and  $\text{Be}_2\text{C}_5$ -III (Fig. 4c), each C atom binds to five Be atoms to form a ppC moiety of  $\text{Be}_5\text{C}$  and the  $\text{Be}_3\text{C}_2$  moieties also can be found in these two isomers.  $\text{Be}_2\text{C}_5$ -I is 50 and 101 meV per atom lower in energy than  $\text{Be}_2\text{C}_5$ -II and  $\text{Be}_2\text{C}_5$ -III, respectively, indicating that  $\text{Be}_2\text{C}_5$ -I is the global minimum

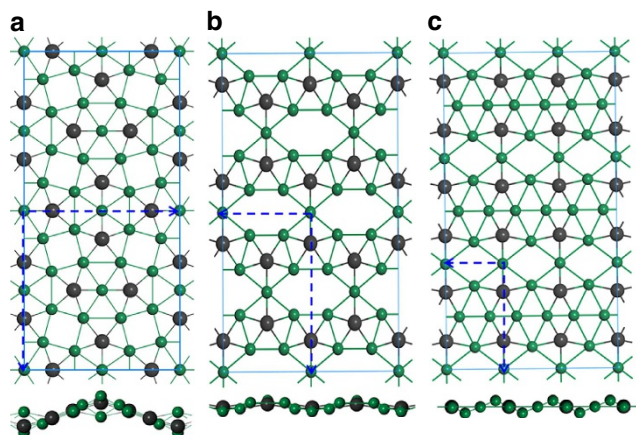


**Figure 4 | Low-energy isomers.** Geometric structures of  $\text{Be}_5\text{C}_2$ -I (a),  $\text{Be}_5\text{C}_2$ -II (b) and  $\text{Be}_5\text{C}_2$ -III (c). The blue dashed lines denote unit cells.

structure in the 2D space. Therefore, the ppC-featuring  $\text{Be}_5\text{C}_2$  monolayer holds great potential to be realized experimentally.

**Electronic properties of  $\text{Be}_5\text{C}_2$  monolayer.** With such interesting structural characteristics, does  $\text{Be}_5\text{C}_2$  monolayer also have intriguing properties? To address this issue, we computed the band structure of the lowest-energy  $\text{Be}_5\text{C}_2$  monolayer. As shown in Fig. 5a,  $\text{Be}_5\text{C}_2$  monolayer is gapless or semi-metallic with the conduction band minimum (CBM) and valence band maximum (VBM) meeting at the Fermi level, which is quite similar to that of graphene. However, the meeting point of  $\text{Be}_5\text{C}_2$  monolayer is located on the path from G (0, 0, 0) point to Y (0, 0.5, 0) point rather than on a high-symmetry point as for graphene. Especially, the conduction and valence bands around the Fermi level exhibit a linear dispersion relation, suggesting that the meeting point of  $\text{Be}_5\text{C}_2$  monolayer is also Dirac-like. Considering that the PBE functional tend to underestimate the band gap, we recomputed the band structure of  $\text{Be}_5\text{C}_2$  monolayer using the hybrid HSE06 functional<sup>56</sup> and found that the dispersion of the valence and conduction bands at the Fermi level is similar to that predicted by PBE and no appreciable band gap can be identified (Supplementary Fig. 5). Thus, the gapless property of  $\text{Be}_5\text{C}_2$  monolayer is solid.

To obtain deeper insight into the electronic properties of  $\text{Be}_5\text{C}_2$  monolayer, we analysed its DOS. As shown in Fig. 5b, the DOS is zero at the Fermi level, which further supports the presence of the Dirac cone. The partial DOS analysis shows that the VBM and CBM are contributed by both Be-2p and C-2p states, and the contribution from Be-2p states is much more than that from C-2p states. Moreover, we plotted the partial charge densities of the VBM and CBM. As shown in Fig. 5c,d, both VBM and CBM are

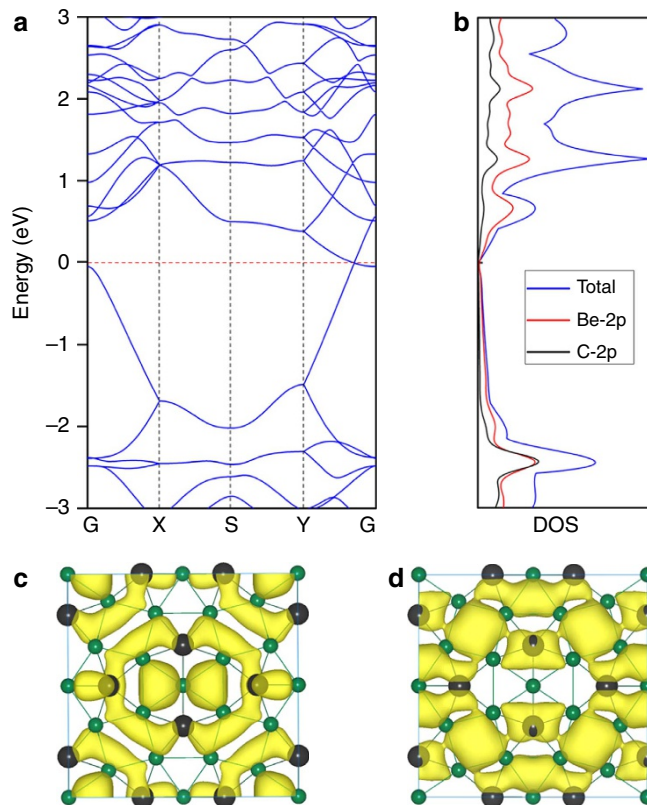


**Figure 5 | Electronic properties of  $\text{Be}_5\text{C}_2$  monolayer.** (a) Band structure and (b) DOS of  $\text{Be}_5\text{C}_2$  monolayer. The Fermi level is assigned at 0 eV. (c,d) The isosurfaces of partial charge densities for the (c) VBM and (d) CBM of  $\text{Be}_5\text{C}_2$  monolayer. The isovalue is  $0.015\text{ e A}^{-3}$ .

mainly originated from the delocalized orbitals of Be atoms and partially from the multicentre bonding between C and Be atoms.

**Mechanical properties of Be<sub>5</sub>C<sub>2</sub> monolayer.** Besides the electronic properties, we also investigated the mechanical properties of Be<sub>5</sub>C<sub>2</sub> monolayer by examining its elastic constants. As a validation, the computed elastic constants of graphene are  $C_{11} = C_{22} = 342.93$  GPa and  $C_{12} = C_{21} = 62.23$  GPa respectively, which achieve good agreements with experimental measurements<sup>57</sup> and previous computations<sup>58</sup>. For Be<sub>5</sub>C<sub>2</sub> monolayer, its elastic constants were computed to be  $C_{11} = 32.90$  GPa,  $C_{22} = 130.89$  GPa,  $C_{12} = C_{21} = -5.32$  GPa and  $C_{66} = 48.32$  GPa, which are in agreement with the mechanical stability criteria for a tetragonal 2D sheet ( $C_{11}C_{22} - C_{12}^2 > 0$ ,  $C_{66} > 0$ )<sup>55</sup>. The in-plane Young's modules along *a* ( $Y_a$ ) and *b* ( $Y_b$ ) directions, which can be deduced from the elastic constants by  $Y_a = (C_{11}C_{22} - C_{12}C_{21})/C_{22}$  and  $Y_b = (C_{11}C_{22} - C_{12}C_{21})/C_{11}$ , were computed to be 32.68 and 130.03 N m<sup>-1</sup>, respectively. As  $Y_a$  is not equal to  $Y_b$ , Be<sub>5</sub>C<sub>2</sub> monolayer is mechanically anisotropic. Moreover, computed at the same level of theory, the in-plane Young's modules of Be<sub>5</sub>C<sub>2</sub> monolayer are less than those of graphene ( $Y_a = Y_b = 331.63$  N m<sup>-1</sup>) but higher than those of phosphorene ( $Y_a = 25.50$  N m<sup>-1</sup> and  $Y_b = 91.61$  N m<sup>-1</sup>), suggesting that Be<sub>5</sub>C<sub>2</sub> monolayer has good mechanical properties.

Remarkably, we noted that Be<sub>5</sub>C<sub>2</sub> monolayer has a negative  $C_{12}$ , which results in negative Poisson's ratios of  $-0.041$  ( $C_{12}/C_{22}$ ) and  $-0.16$  ( $C_{12}/C_{11}$ ) for *a* and *b* directions, respectively. It is noteworthy that the Poisson's ratio is defined as the negative ratio of transverse to axial strain. The negative Poisson's ratio indicates that Be<sub>5</sub>C<sub>2</sub> monolayer can be compressed or stretched in both two directions at the same time. For a validation, we applied a uniaxial strain of 5% in *a* and *b* directions of Be<sub>5</sub>C<sub>2</sub> monolayer, respectively. Just as expected, the equilibrium lattice parameters of *b* and *a* directions are elongated by  $\sim 0.2$  and  $\sim 0.8\%$ , respectively, confirming that Be<sub>5</sub>C<sub>2</sub> monolayer indeed has negative Poisson's ratios.

## Discussion

The unusual negative Poisson's ratio may endow Be<sub>5</sub>C<sub>2</sub> monolayer with enhanced toughness and shear resistance, as well as enhanced sound and vibration adsorption. Correspondingly, Be<sub>5</sub>C<sub>2</sub> monolayer could find some important applications in the fields of mechanics, tissue engineering and national security. It is worth noting that the negative Poisson's ratio is rather peculiar, as in nature nearly all materials have a positive Poisson's ratio, except some so-called auxetic materials<sup>59</sup>. Recently, Jiang *et al.*<sup>60</sup> demonstrated theoretically that single-layer black phosphorus has a negative Poisson's ratio due to the unique puckered configuration. However, the negative Poisson's ratio of phosphorene was observed in the out-of-plane direction, which is different from that of Be<sub>5</sub>C<sub>2</sub> monolayer. Remarkably, the Poisson's ratio of Be<sub>5</sub>C<sub>2</sub> monolayer in the *b* direction ( $-0.16$ ) is much higher than that of phosphorene ( $-0.027$ )<sup>60</sup>, rendering Be<sub>5</sub>C<sub>2</sub> monolayer a more promising candidate for specific application in mechanical devices. No doubt, the negative Poisson's ratio of Be<sub>5</sub>C<sub>2</sub> monolayer should be originated from its intriguing structural properties, especially the uniquely oriented chemical bonds. Our results could provide some guidelines for designing materials with a negative Poisson's ratio.

With so many fascinating properties, it is desirable to synthesize Be<sub>5</sub>C<sub>2</sub> monolayer in the laboratory. Considering that there is no layered structure of Be<sub>5</sub>C<sub>2</sub> in nature, a promising approach is to grow Be<sub>5</sub>C<sub>2</sub> monolayer on the surface of metal or metal oxide via chemical vapour deposition with accurately controlled Be/C ratio, just similar to the growth of silicene<sup>47,48</sup>. It

is noteworthy that Be has toxic properties and the chemical vapour deposition synthesis usually requires high temperature; hence, special caution should be given during the experimental realization.

To summarize, inspired by the bonding characters of a ppC-containing molecule, Be<sub>9</sub>C<sub>2</sub><sup>4-</sup>, we designed a ppC-containing 2D inorganic material with a Be<sub>5</sub>C<sub>2</sub> stoichiometry. Our DFT computations demonstrated that ppCs in Be<sub>5</sub>C<sub>2</sub> monolayer are essentially stabilized by the charge transfer from Be ligands. The moderate cohesive energy, absence of imaginary modes in phonon spectrum and high melting point evaluated from FPMD simulations indicated that Be<sub>5</sub>C<sub>2</sub> monolayer is experimentally viable. Especially, a global minimum search revealed that Be<sub>5</sub>C<sub>2</sub> monolayer is the lowest-energy structure for the Be<sub>5</sub>C<sub>2</sub> stoichiometry in 2D space, which endows Be<sub>5</sub>C<sub>2</sub> monolayer great possibility to be realized experimentally. Our computations demonstrated that Be<sub>5</sub>C<sub>2</sub> monolayer is semi-metallic with a zero band gap in the electronic band structure. More interestingly, Be<sub>5</sub>C<sub>2</sub> monolayer has rather intriguing mechanical properties featured with a negative Poisson's ratio. Therefore, Be<sub>5</sub>C<sub>2</sub> monolayer is expected to have wide applications in electronics and mechanics. We hope our theoretical studies will promote the experimental realization of this novel material and attract more attentions on investigating nanomaterials with novel chemical bonding.

## Methods

**DFT computations.** For the Be<sub>9</sub>C<sub>2</sub><sup>4-</sup> molecule, geometry optimizations, frequency analyses and electronic structure computations were performed at the B3LYP<sup>61,62</sup> level of theory with the 6-311 + G\*(*d*, *p*) basis set as implemented in Gaussian 03 package<sup>63</sup>. For 2D Be<sub>5</sub>C<sub>2</sub> monolayer, DFT computations were performed using the plane-wave technique implemented in Vienna *ab initio* simulation package<sup>64</sup>. The ion-electron interaction was described using the projector-augmented plane wave approach<sup>65,66</sup>. The generalized gradient approximation expressed by PBE functional<sup>67</sup> and a 500-eV cutoff for the plane-wave basis set were adopted in all the computations. The convergence threshold was set as  $10^{-4}$  eV in energy and  $10^{-3}$  eV Å<sup>-1</sup> in force. We set the *x* and *y* directions parallel and the *z* direction perpendicular to the layer plane, and adopted a supercell length of 15 Å in the *z* direction. The Brillouin zones was sampled with an  $8 \times 6 \times 1$  *I* centred *k* points grid. The phonon spectrum was computed using finite displacement method as implemented in CASTEP code<sup>68</sup>. The elastic constants were also computed using the CASTEP code. The chemical bonding analysis of Be<sub>5</sub>C<sub>2</sub> monolayer was done using the SSAAdNDP method<sup>46</sup>, which can well interpret the chemical bonding in terms of classical lone pairs, two-centre bonds, as well as multi-centre delocalized bonds in bulk solids, surfaces and nanostructures.

**Molecular dynamics simulations.** The thermal stability of Be<sub>5</sub>C<sub>2</sub> monolayer was evaluated by means of first-principles molecular dynamics simulations. The ground-state structure of Be<sub>5</sub>C<sub>2</sub> monolayer was annealed at different temperatures. At each temperature, MD simulation in NVT ensemble lasts for 10 ps with a time step of 1.0 fs. The temperature was controlled by using the Nosé-Hoover method<sup>69</sup>.

**Global minimum structure searches.** The PSO method within the evolutionary scheme as implemented in the CALYPSO code<sup>70</sup> was employed to find the low-energy structures of 2D Be<sub>5</sub>C<sub>2</sub> monolayer. In our PSO simulation, the number of generation was maintained at 30. Unit cells containing total atoms of 7, 14 and 28 were considered. The structure relaxations during the PSO simulation were performed using Vienna *ab initio* simulation package at PBE level of theory.

**Data availability.** All relevant data are available from the authors.

## References

- van'tHoff, J. H. On the structure formulas in three-dimensional space. *Arch. Neerl. Sci. Exactes Nat.* 445–454 (1874).
- LeBel, J. A. Sur les relations qui existent entre les formules atomiques des coprs organique et le pouvoir de leurs dissolutions. *Bull. Soc. Chim. Fr.* 22, 337–347 (1874).
- Monkhorst, H. J. Activation energy for interconversion of enantiomers containing an asymmetric carbon atom without breaking bonds. *Chem. Commun.* 1111–1112 (1968).
- Hoffmann, R., Alder, R. W. & Wilcox, Jr C. F. Planar tetracoordinate carbon. *J. Am. Chem. Soc.* 92, 4992–4993 (1970).

5. Collins, J. B. *et al.* Stabilization of planar tetracoordinate carbon. *J. Am. Chem. Soc.* **98**, 5419–5427 (1976).
6. Cotton, F. A. & Millar, M. M. The probable existence of a triple bond between two vanadium atoms. *J. Am. Chem. Soc.* **99**, 7886–7891 (1977).
7. Keese, R. Carbon flatland: planar tetracoordinate carbon and fenestranes. *Chem. Rev.* **106**, 4787–4808 (2006).
8. Merino, G., Méndez-Rojas, M. A., Vela, A. & Heine, T. Recent advances in planar tetracoordinate carbon chemistry. *J. Comput. Chem.* **28**, 362–372 (2007).
9. Yang, L.-M., Ganz, E., Chen, Z., Wang, Z.-X. & Schleyer, P. v. R. Four decades of the chemistry of planar hypercoordinate compounds. *Angew. Chem. Int. Ed.* **54**, 9468–9501 (2015).
10. Krogh-Jespersen, M.-B., Chandrasekhar, J., Wuerthwein, E.-U., Collins, J. B. & Schleyer, P. v. R. Molecular orbital study of tetrahedral, planar, and pyramidal structures of the isoelectronic series  $\text{BH}_4^-$ ,  $\text{CH}_4$ ,  $\text{NH}_4^+$ ,  $\text{AlH}_4^-$ ,  $\text{SiH}_4$ , and  $\text{PH}_4^+$ . *J. Am. Chem. Soc.* **102**, 2263–2268 (1980).
11. Boldyrev, A. I. & Simons, J. Tetraordinated planar carbon in pentaatomic molecules. *J. Am. Chem. Soc.* **120**, 7967–7972 (1998).
12. Merino, G., Méndez-Rojas, M. A. & Vela, A.  $(\text{C}_5\text{M}_2\text{-n})^{n-}$  (M = Li, Na, K, and n = 0, 1, 2). A new family of molecules containing planar tetracoordinate carbons. *J. Am. Chem. Soc.* **125**, 6026–6027 (2003).
13. Merino, G. *et al.* Theoretical analysis of the smallest carbon cluster containing a planar tetracoordinate carbon. *J. Am. Chem. Soc.* **126**, 16160–16169 (2004).
14. Wang, Z. X., Zhang, C. G., Chen, Z. F. & Schleyer, P. v. R. Planar tetracoordinate carbon species involving beryllium substituents. *Inorg. Chem.* **47**, 1332–1336 (2008).
15. Wu, Y. B., Lu, H. G., Li, S. D. & Wang, Z. X. Simplest neutral singlet  $\text{C}_2\text{E}_4$  (E = Al, Ga, In, and Tl) global minima with double planar tetracoordinate carbons: equivalence of  $\text{C}_2$  moieties in  $\text{C}_2\text{E}_4$  to carbon centers in  $\text{CAL}_4^{2-}$  and  $\text{CAL}_5^+$ . *J. Phys. Chem. A* **113**, 3395–3402 (2009).
16. Li, X., Zhang, H.-F., Wang, L.-S., Boldyrev, A. I. & Simons, J. Tetraordinated planar carbon in the  $\text{Al}_4\text{C}^-$  Anion: a combined photoelectron spectroscopy and *ab initio* study. *J. Am. Chem. Soc.* **121**, 6033–6038 (1999).
17. Li, X., Zhang, H.-F., Wang, L.-S., Geske, G. D. & Boldyrev, A. I. Pentaatomic tetracoordinate planar carbon,  $[\text{CAL}_4]^{2-}$ : a new structural unit and its salt complexes. *Angew. Chem. Int. Ed.* **39**, 3630–3632 (2000).
18. Wang, L.-S., Boldyrev, A. I., Li, X. & Simons, J. Experimental observation of pentaatomic tetracoordinate planar carbon-containing molecules. *J. Am. Chem. Soc.* **122**, 7681–7687 (2000).
19. Wang, Z.-X. & Schleyer, P. v. R. Construction principles of “hyparenes”: families of molecules with planar pentacoordinate carbons. *Science* **292**, 2465–2469 (2001).
20. Pei, Y., An, W., Ito, K., Schleyer, P. v. R. & Zeng, X. C. Planar pentacoordinate carbon in  $\text{CAL}_5^+$ : a global minimum. *J. Am. Chem. Soc.* **130**, 10394–10400 (2008).
21. Jimenez-Halla, J. O. *et al.*  $\text{CAL}_4\text{Be}$  and  $\text{CAL}_3\text{Be}_2^-$ : global minima with a planar pentacoordinate carbon atom. *Chem. Commun.* **46**, 8776–8778 (2010).
22. Grande-Aztatzi, R. *et al.* Planar pentacoordinate carbons in  $\text{CBe}_5^{4-}$  derivatives. *Phys. Chem. Chem. Phys.* **17**, 4620–4624 (2015).
23. Exner, K. & Schleyer, P. v. R. Planar hexacoordinate carbon: a viable possibility. *Science* **290**, 1937–1940 (2000).
24. Ito, K. *et al.* Myriad planar hexacoordinate carbon molecules inviting synthesis. *J. Am. Chem. Soc.* **129**, 1510–1511 (2007).
25. Wang, Z.-X. & Schleyer, P. v. R. Planar hypercoordinate carbons joined: wheel-shaped molecules with C–C axes. *Angew. Chem. Int. Ed.* **41**, 4082–4085 (2002).
26. Pancharatna, P. D., Méndez-Rojas, M. A., Merino, G., Vela, A. & Hoffmann, R. Planar tetracoordinate carbon in extended systems. *J. Am. Chem. Soc.* **126**, 15309–15315 (2004).
27. Yang, L. M., Ding, Y. H. & Sun, C. C. Design of sandwich-like complexes based on the planar tetracoordinate carbon unit  $\text{CAL}_4^{2-}$ . *J. Am. Chem. Soc.* **129**, 658–665 (2007).
28. Zhang, C. J., Sun, W. X. & Cao, Z. X. Zigzag boron-carbon nanotubes with quasi-planar tetracoordinate carbons. *J. Am. Chem. Soc.* **130**, 5638–5639 (2008).
29. Wu, M.-H., Pei, Y. & Zeng, X. C. Planar tetracoordinate carbon strips in edge decorated graphene nanoribbon. *J. Am. Chem. Soc.* **132**, 5554–5555 (2010).
30. Wu, Y. B., Jiang, J. L., Zhang, E. W. & Wang, Z. X. Computationally designed families of flat, tubular, and cage molecules assembled with “starbenzene” building blocks through hydrogen-bridge bonds. *Chem. Eur. J.* **16**, 1271–1280 (2010).
31. Novoselov, K. S. *et al.* A roadmap for graphene. *Nature* **490**, 192–200 (2012).
32. Tang, Q., Zhou, Z. & Chen, Z. Graphene-related nanomaterials: tuning properties by functionalization. *Nanoscale* **5**, 4541–4583 (2013).
33. Xu, M. S., Liang, T., Shi, M. & Chen, H. Graphene-like two-dimensional materials. *Chem. Rev.* **113**, 3766–3798 (2013).
34. Tang, Q., Zhou, Z. & Chen, Z. Innovation and discovery of graphene-like materials via density functional theory computations. *WIREs Comput. Mol. Sci.* **5**, 360–379 (2015).
35. Wu, X. J., Pei, Y. & Zeng, X. C.  $\text{B}_2\text{C}$  graphene, nanotubes, and nanoribbons. *Nano Lett.* **9**, 1577–1582 (2009).
36. Li, Y., Liao, Y., Schleyer, P. v. R. & Chen, Z.  $\text{Al}_2\text{C}$  monolayer: the planar tetracoordinate carbon global minimum. *Nanoscale* **6**, 10784–10791 (2014).
37. Dai, J., Wu, X., Yang, J. & Zeng, X.  $\text{Al}_3\text{C}$  monolayer sheets: two-dimensional networks with planar tetracoordinate carbon and potential applications as donor materials in solar cell. *J. Phys. Chem. Lett.* **5**, 2058–2065 (2014).
38. Zhang, Z., Liu, X., Yakobson, B. I. & Guo, W. Two-dimensional tetragonal TiC monolayer sheet and nanoribbons. *J. Am. Chem. Soc.* **133**, 19326–19329 (2012).
39. Li, Y., Li, F., Zhou, Z. & Chen, Z.  $\text{SiC}_2$  silagraphene and its one-dimensional derivatives: where planar tetracoordinate silicon happens. *J. Am. Chem. Soc.* **133**, 900–908 (2011).
40. Yang, L.-M. *et al.* Two-dimensional  $\text{Cu}_2\text{Si}$  monolayer with planar hexacoordinate copper and silicon bonding. *J. Am. Chem. Soc.* **137**, 2757–2762 (2015).
41. Yang, L.-M. *et al.* Revealing unusual chemical bonding in planar hyper-coordinate  $\text{Ni}_2\text{Ge}$  and quasi-planar  $\text{Ni}_2\text{Si}$  two-dimensional crystals. *Phys. Chem. Chem. Phys.* **17**, 26043–26048 (2015).
42. Yang, L.-M. *et al.* Post-anti-van’t Hoff-Le Bel motif in atomically thin germanium ally film. *Phys. Chem. Chem. Phys.* **17**, 17545–17551 (2015).
43. Pei, Y. & Zeng, X. C. Probing the planar tetra-, penta-, and hexacoordinate Carbon in carbon-boron mixed clusters. *J. Am. Chem. Soc.* **130**, 2580–2592 (2008).
44. Luo, X. *et al.* Predicting two-dimensional boron-carbon compounds by the global optimization method. *J. Am. Chem. Soc.* **133**, 16285–16290 (2011).
45. Li, Y., Liao, Y. & Chen, Z.  $\text{Be}_2\text{C}$  monolayer with quasi-planar hexacoordinate carbons: a global minimum structure. *Angew. Chem. Int. Ed.* **53**, 7248–7252 (2014).
46. Galeev, T. R., Dunnington, B. D., Schmidt, J. R. & Boldyrev, A. I. Solid state adaptive natural density partitioning: a tool for deciphering multi-center bonding in periodic systems. *Phys. Chem. Chem. Phys.* **15**, 5022–5029 (2013).
47. Feng, B. J. *et al.* Evidence of silicene in honeycomb structures of silicon on Ag (111). *Nano Lett.* **12**, 3507–3511 (2012).
48. Fleurence, A. *et al.* Experimental evidence for epitaxial silicene on diboride thin films. *Phys. Rev. Lett.* **108**, 245501 (2012).
49. Li, L. *et al.* Black phosphorus field-effect transistors. *Nat. Nanotechnol.* **9**, 372–377 (2014).
50. Liu, H., Neal, A. T., Zhu, Z., Tomanek, D. & Ye, P. D. Phosphorene: an unexplored 2D semiconductor with a high hole mobility. *ACS Nano* **8**, 4033–4041 (2014).
51. Molina-Sánchez, A. & Wirtz, L. Phonons in single-layer and few-layer  $\text{MoS}_2$  and  $\text{WS}_2$ . *Phys. Rev. B* **84**, 155413 (2011).
52. Cahangirov, S., Topsakal, M., Akturk, E., Sahin, H. & Ciraci, S. Two- and one-dimensional honeycomb structures of silicon and germanium. *Phys. Rev. Lett.* **102**, 236804 (2009).
53. Terrones, H. *et al.* New metallic allotropes of planar and tubular carbon. *Phys. Rev. Lett.* **84**, 1716 (2000).
54. Liu, Y., Wang, G., Huang, Q., Guo, L. & Chen, X. Structural and electronic properties of t-graphene: a two-dimensional carbon allotrope with tetrarings. *Phys. Rev. Lett.* **108**, 225505 (2012).
55. Zhang, S. *et al.* Penta-graphene: a new carbon allotrope. *Proc. Natl Acad. Sci. USA* **112**, 2372–2377 (2015).
56. Heyd, J., Scuseria, G. E. & Ernzerhof, M. Erratum: “Hybrid functionals based on a screened Coulomb potential”. *J. Chem. Phys.* **124**, 219906 (2006).
57. Lee, C. G., Wei, X. D., Kysar, J. W. & Hone, J. Measurement of the elastic properties and intrinsic strength of monolayer graphene. *Science* **321**, 385–388 (2008).
58. Li, X., Zhang, Q. & Wang, Q. Stability and physical properties of a tri-ring based porous  $\text{gC}_4\text{N}_3$  sheet. *Phys. Chem. Chem. Phys.* **15**, 7142–7146 (2013).
59. Lakes, R. S. Foam structures with a negative Poisson’s ratio. *Science* **235**, 1038–1040 (1987).
60. Jiang, J.-W. & Park, H. S. Negative Poisson’s ratio in single-layer black phosphorus. *Nat. Commun.* **5**, 4727 (2014).
61. Becke, A. D. Density-functional thermochemistry. III. The role of exact exchange. *J. Chem. Phys.* **98**, 5648–5652 (1993).
62. Lee, C., Yang, W. & Parr, R. G. Development of the colle-salvetti correlation-energy formula into a functional of the electron density. *Phys. Rev. B: Condens. Mater. Phys.* **37**, 785 (1988).
63. Frisch, M. J. *et al.* GAUSSIAN 03, Revision E.02 (Gaussian, Inc., 2004).
64. Kresse, G. & Hafner, J. Ab initio molecular dynamics for liquid metals. *Phys. Rev. B* **47**, 558 (1993).
65. Blöchl, P. E. Projector augmented-wave method. *Phys. Rev. B* **50**, 17953–17979 (1994).
66. Kresse, G. & Joubert, D. From ultrasoft pseudopotentials to the projector augmented-wave method. *Phys. Rev. B* **59**, 1758 (1999).
67. Perdew, J. P., Burke, L. & Ernzerhof, M. Generalized gradient approximation made simple. *Phys. Rev. Lett.* **77**, 3865 (1996).

68. Segall, M. D. *et al.* First-principles simulation: ideas, illustrations and the CASTEP code. *J. Phys. Condens. Matter* **14**, 2717 (2002).
69. Martyna, G. J., Klein, M. L. & Tuckerman, M. E. Nosé-Hoover chains: the canonical ensemble via continuous dynamics. *J. Chem. Phys.* **97**, 2635–2643 (1992).
70. Wang, Y., Lv, J., Zhu, L. & Ma, Y. Crystal structure prediction via particle-swarm optimization. *Phys. Rev. B* **82**, 094116 (2010).

### Acknowledgements

Support in China by Natural Science Foundation of China (numbers 21403115 and 21522305) and the NSF of Jiangsu Province of China (number BK20150045), and in the United States by National Science Foundation (Grant EPS-1010094) and Department of Defense (Grant W911NF-12-1-0083) is gratefully acknowledged. The computational resources used in this research were provided by Shanghai Supercomputer Center.

### Author contributions

Y.L. and Z.C. conceived the initial idea of this research. Y.W. and F.L. demonstrated the initial idea and collected all the data. Y.W., Y.L. and Z.C. wrote the paper and all authors commented on it.

### Additional information

**Supplementary Information** accompanies this paper at <http://www.nature.com/naturecommunications>

**Competing financial interests:** The authors declare no competing financial interests.

**Reprints and permission** information is available online at <http://npg.nature.com/reprintsandpermissions/>

**How to cite this article:** Wang, Y. *et al.* Semi-metallic Be<sub>5</sub>C<sub>2</sub> monolayer global minimum with quasi-planar pentacoordinate carbons and negative Poisson's ratio. *Nat. Commun.* **7**:11488 doi: 10.1038/ncomms11488 (2016).



This work is licensed under a Creative Commons Attribution 4.0 International License. The images or other third party material in this article are included in the article's Creative Commons license, unless indicated otherwise in the credit line; if the material is not included under the Creative Commons license, users will need to obtain permission from the license holder to reproduce the material. To view a copy of this license, visit <http://creativecommons.org/licenses/by/4.0/>